Antimicrobial and Biofilm-Inhibitory Potential of Green Synthesized Silver Nanoparticles from *Lantana camara* against *Pseudomonas aeruginosa*

Achal Dharmalal Rajratna, Saurav K. Saha, Tapas K. Sengupta*

Department of Biological Sciences

Indian Institute of Science Education and Research Kolkata

Mohanpur, Nadia- 741 246, West Bengal, India

***Email: senguptk@iiserkol.ac.in**

Abstract

Emerging antimicrobial resistance has been a serious threat to human well-being. Current therapeutics face several drawbacks while treating bacterial infections because of the bacteria's ability to attach to various surfaces and form biofilm as a defence mechanism. One such pathogen, *Pseudomonas aeruginosa*, can form biofilm for its survival in the presence of various antibacterial agents. The present study explores the efficacy of green synthesized silver nanoparticles against bacteria, mainly against *Pseudomonas aeruginosa*, where *Lantana camara* leaf extract contributes as a reducing agent to reduce Ag^{+} to Ag^{0}.

UV-vis spectroscopy of the nanoparticle showed a maximum spectrum at 416 nm, while dynamic light scattering revealed the size to be 30-35nm. The size and morphology of the nanoparticle were confirmed by various electron microscopies. The synthesized nanoparticles revealed significant antibacterial and antibiofilm activity against *Pseudomonas aeruginosa* environmental isolates KPW.1-S1 and HRW.1-S3. Further, microscopic analyses through confocal and scanning electron microscopy validated the reduction in biofilm. Importantly, the cytotoxic effect of the nanoparticle on Human Kidney Epithelial-like cells was checked, and it revealed no significant toxicity. Therefore, *Lantana camara* silver conjugated nanoparticles provide an eco-friendly alternative to

traditional antimicrobials, highlighting their potential for combating multidrug-resistant infection while ensuring mammalian cell safety.

Keywords: Antibacterial activity, Biofilm, Green synthesized nanoparticles, *Lantana camara*, *Pseudomonas aeruginosa*

1. Introduction

Pseudomonas aeruginosa (PA), Gram-negative, rod-shaped bacteria, are well-known opportunistic pathogens widely found in water, soil, plants, and animals, including humans. These pathogens are essential to study due to their inherent ability to form biofilm on different surfaces under adverse conditions as a defence mechanism and for its survival, making it clinically relevant. *Pseudomonas aeruginosa* causes secondary infections in immunosuppressed individuals as well as patients who have cystic fibrosis (1,2), chronic wounds (3), mastitis (4), endometritis (5), and thermal wounds (6). As stated in reports by the Centers for Disease Control (CDC) and Prevention experts, it is estimated that about 65% of human bacterial infections are linked to biofilms, highlighting their impact on health and the challenges they pose for treatment (7,8).

Pseudomonas aeruginosa isolates are generally used as model organisms for biofilm-related studies as they are avid biofilm formers, causing chronic infections (8). Besides the site of infections, PA can grow as biofilm on a variety of surfaces, including medical implants and catheters, making it clinically more vital. Biofilm also helps bacteria avoid phagocytosis and defend against different constituents of the host's adaptive and innate immune systems, making it resistant to antimicrobial treatments (8). It is reported that antimicrobial resistance (AMR) was heightened in biofilm cells compared to planktonic cells (9,10). Thus, the increasing mortality and antimicrobial resistance of *Pseudomonas aeruginosa* highlight the need to develop novel therapeutics against the bacteria for combating these infections.

Different novel strategies are being developed against *Pseudomonas* infections in recent times due to their ability to develop new resistance mechanisms to existing strategies. Newer strategies such as anti-quorum sensing molecules, synthetic small organic molecules (11), antibiofilm peptides

(12), matrix-degrading enzymes (13), phage therapy (14), and CRISPR-Cas9 (15), photodynamic therapies (16), vaccines (17), nanoparticles and biomaterials (18) are in use to enhance treatment effectiveness against infections associated with biofilms. Nanoparticles, in particular, have been an emerging tool in the recent field of therapeutics.

Nanotechnology-based tools have several advantages over different novel therapeutics, such as a high surface area to volume ratio, reactivity, and stability (19). These nanotechnologies have shown a positive impact in the field of biomedicine and pharmaceuticals, due to their effectiveness in reducing infections with conventional drug administration methods (20). Synthesis of nanoparticles through chemical synthesis involves an energy-intensive process with harsh chemical involvement, which can be overridden by green synthesis of nanoparticles, as this method offers non-toxic plant extract involvement, which acts as a reducing agent (21). The green synthesized nanoparticles can be produced on a large scale with an eco-friendly approach. The involvement of biological components in a reducing and capping agent avoids high energy and pressure needs and, simultaneously less hazardous than chemically synthesized counterparts (22,23). Among different types of nanoparticles, green synthesized metal-based nanoparticles have exhibited good potential as antimicrobial agents (24), antifungal agents (25), and also as anticancer agents (25,26).

Silver nanoparticles have been recognized for their potent antibacterial properties, effectively targeting both Gram-negative and Gram-positive bacterial strains (27,28). Silver nanotechnology can potentially inhibit bacterial infections by following the mode of action as cell membrane damage, producing different types of reactive oxygen species (ROS), and inhibiting enzymes (29,30). Such green synthesized silver nanoparticles are known to be effective, and they have many potential applications (31).

Lantana camara, an invasive, adaptable weed native to the American tropics, is a flowering plant of the Verbenaceae family. It has spread across the world, including India. *L. camara* has been used in traditional medicine to treat various diseases (32). Different studies have found that *L. camara* leaves display bactericidal, insecticidal, fungicidal, nematocidal, antioxidant, and anticancer properties (33,34). Traditionally, various parts of this plant, like flowers, leaves, and roots, have been utilized in herbal medicine (35). Bioactive compounds present in the plant have

been found to have antibacterial activity. As only a tiny fraction of plant species has been thoroughly investigated for their therapeutic benefits, deep research into the potential of *L. camara* as an antimicrobial agent may lead to the discovery of novel treatments that are both effective and less toxic than current chemotherapeutic agents.

Metallic nanoparticles have been investigated over the past few years, and it has demonstrated the potential against clinically relevant pathogens, including *P. aeruginosa* (36,37). Yadav et al. showed that silver nanoparticles are quite effective in inhibiting *PA* biofilms (38). Though metal-based nanoparticles have promise, their toxicity limits their uses (39). Thus, green synthesis approaches have shown a promising alternative for PA infection due to their eco-friendly, less toxic and biocompatible nature (21). Various biosynthesized nanoparticles were also found to be effective against biofilm formation, as well as the virulence genes of PA (40). *Lantana camara* conjugated silver nanoparticles were also found to have an antibacterial effect on various bacteria (41). Although these studies confirm the antibacterial potential of the *Lantana camara* conjugated silver nanoparticles, their antibiofilm potential has not yet been explored in depth.

Hence, in the current study, we have synthesized *Lantana camara* leaf extract conjugated silver nanoparticles (LCLE-Ag NPs) and have characterized them using various techniques. Additionally, we have evaluated the antimicrobial and anti-biofilm properties of the prepared nanoparticles against two environmental strains of *Pseudomonas aeruginosa,* KPW.1-S1 and HRW.1-S3, which were isolated from contaminated water sources and found to express various virulent genes (42).

2. Materials and Methods

2.1. Bacterial strains of *Pseudomonas aeruginosa*

The *Pseudomonas aeruginosa* strains KPW.1-S1 and HRW.1-S3 were isolated from Kolkata Port water and Haldi River water, respectively (43) and further identified by 16S rRNA sequencing (NCBI Accession numbers FJ897721 and FJ897723 respectively). The strains were deposited at the Microbial Type Culture Collection and Gene Bank (MTCC), Chandigarh, India, under the catalogue numbers MTCC 10087 and MTCC 10088 (43).

For growth, *P. aeruginosa* KPW.1-S1 and HRW.1-S3 were inoculated and grown in a modified Bushnell-Haas (BH) medium supplemented with 2% glucose as the carbon source (44).

2.2 Cell Culture of HEK293T cells

The HEK293T (human kidney epithelial-like) cell line was obtained from the National Centre for Cell Science, Pune, India. The cell line was maintained in Dulbecco's Modified Eagle Medium (DMEM) High Glucose (HiMedia, India), supplemented with 10% Fetal Bovine Serum (FBS) (HiMedia, India), 10000 U/mL Penicillin, and 10 mg/mL Streptomycin antibiotic solution (HiMedia, India). Cells were maintained at 37 °C in a humidified environment with 5% CO_2 and 95% air to ensure optimal growth conditions (35).

2.3. *Lantana camara* leaf extract (LCLE) preparation

The leaf extract was prepared following the protocol described by Pal et al. (35), with slight modifications. Healthy *L. camara* leaves were collected from the Indian Institute of Science Education and Research, Kolkata campus (22°57′50″N, 88°31′28″E). The leaves were taxonomically verified by the Central National Herbarium, Botanical Survey of India (West Bengal, India), with a voucher reference number IISER/AP/01. Then they were thoroughly washed with water and then shade-dried for 48 hours. The dried leaves were powdered using a mortar and pestle for subsequent processing.

Leaf powder was extracted with absolute ethanol (Merck) at a 1:10 w/v ratio at 37 °C for 18 hours in a shaker. The extract was filtered, concentrated by a rotary evaporator, reconstituted in molecular-grade ethanol (Merck, Germany), sterilized through a syringe filter (HiMedia) of pore size 0.22-µm, and stored at 4 °C.

2.4. Synthesis of silver nanoparticles

A 2 mg/mL solution of ethanol-based leaf extract of *L. camara* dispersed in water and a 3 mM silver nitrate solution were mixed in a conical flask in a 2:1 ratio. The silver nitrate solution was added dropwise over the course of one hour. It was then incubated in a hot water bath at 60 °C for three hours until the solution turned brownish-yellow. The resulting mixture was centrifuged

(13,000 rpm,10 minutes), and the pellet was resuspended in water and stored at 4 °C for further use (41).

2.5. Characterization of Nanoparticles

2.5.1. Ultraviolet-visible spectroscopy of LCLE-Ag NPs

The synthesized nanoparticles were analyzed using a UV-Vis spectrophotometer (Beckman Coulter DU 730). The analysis was conducted in the wavelength range of 200–800 nm, utilizing continuous scanning mode to capture detailed spectral data. Distilled water was employed as a blank.

2.5.2. Dynamic Light Scattering and Zeta Potential of LCLE-Ag NPs

The polydispersity index (PDI), average particle size, and zeta potential were measured using a Zetasizer (Nano ZS, Malvern) using DLS. The samples were prepared by dispersing them with sonication and diluting them with MiliQ water as required.

2.5.3 Scanning Electron Microscopy and Energy-Dispersive X-ray spectroscopy of LCLE-Ag NPs

The morphological characteristics and elemental composition of the synthesized LCLE-Ag NPs were studied using field emission scanning electron microscopy (FESEM) integrated with energy-dispersive X-ray spectroscopy (EDX) (Supra 55 VP, Carl Zeiss). The nanoparticle was drop-cast on cover slips, then mounted on aluminium stubs for SEM analysis, and *L. camara* powdered leaf extract was directly mounted on stubs for EDX analysis. The samples were subjected to sputter coating and subsequently analyzed under the electron microscope.

2.5.4. Transmission Electron Microscopy of LCLE-Ag NPs

Transmission electron microscopy (TEM) (JEM-2100 Plus, JEOL) was performed to determine the size of the nanoparticles. Samples were drop-cast on a carbon-coated copper grid, which was then left to air-dry overnight. The samples were desiccated and visualized under TEM at an accelerating voltage of 300 kV.

2.5.5. Atomic Force Microscopy of LCLE-Ag NPs

To prepare the LCLE-Ag NP sample for examination using Atomic Force Microscopy (AFM) (Cypher asylum Research AFM, Oxford Instruments), the nanoparticle was drop-cast on a silicon wafer and was placed on a tissue paper-lined petri dish, allowed to air dry in a laminar flow hood. Afterwards, the air-dried silicon wafer was desiccated and then examined under the microscope.

2.5.6. Attenuated Total Reflectance (ATR) FTIR of LCLE-Ag NPs

ATR was used to examine the presence of functional groups in the nanoparticles and *L. camara* leaf extract powdered samples. ATR was performed using a PerkinElmer Spectrum RX1 spectrophotometer in the scanning range of 500-4500 cm^{-1}.

2.6. Minimum Inhibitory Concentration (MIC) assay

The MIC assay was used to evaluate the minimal inhibitory concentration of LCLE-Ag NPs against two different strains of *Pseudomonas aeruginosa*, namely KPW.1-S1 and HRW.1-S3. Various concentrations of LCLE-Ag NPs (5- 10- 20- 50- 100 µg/mL) were prepared and added to bacterial cultures. The individual bacterial cultures treated with nanoparticles were incubated in a shaker (37 °C, 150 rpm) along with their respective blanks. Following 18 hours of incubation, the optical density (OD) was measured using a UV-Vis spectrophotometer (Schimadzu) at 600 nm.

2.7. Quantification of *Pseudomonas aeruginosa* Biofilm

The biofilm load assay was performed on 24-well plates coated with polystyrene (NUNC). 3 x 10^6 cells/mL of *Pseudomonas aeruginosa* KPW.1-S1 and HRW.1-S3 were individually cultured with different concentrations of LCLE-Ag NPs in an orbital shaker (37 °C, 150 rpm). After 24 hours, the optical density of the planktonic cells was measured at 600nm using a UV-Vis spectrophotometer. The wells were rinsed twice with Phosphate Buffered Saline (PBS) to remove any excess planktonic cells, followed by staining the wells with 0.1% Crystal violet (CV) for 45 minutes. Post incubation, the CV was discarded and the wells were washed twice with PBS again. Then, 1 mL of 30% acetic acid was added to each well, and the plates were kept in the shaker (37 °C, 150 rpm) for 30 minutes to solubilize the stain. The optical density of the solubilized crystal violet was measured using a plate reader at 600 nm (BioTek ELx800).

2.8. Scanning Electron Microscopy of *Pseudomonas aeruginosa* biofilm

The *Pseudomonas aeruginosa* KPW.1-S1 and HRW.1-S3 biofilm was grown on a glass coverslip in 24-well plates. After the 24-hour incubation period, each coverslip was washed twice with PBS to remove any planktonic cells. The coverslips were then immersed in 2.5% glutaraldehyde for 2 hours at 4 °C in the dark to fix the biofilm structure. Then they were washed thrice with PBS. Next, the coverslips were treated with 0.1% osmium tetroxide for 45 minutes at 4 °C in the dark. After another series of three PBS washes, the coverslips were subjected to a dehydration process using an alcohol gradient from 30% to 100%, with each concentration applied for 10 minutes. Finally, the coverslips were dried under a vacuum in a desiccator and examined in Scanning Electron Microscopy using Carl Zeiss smart software for detailed analysis of the biofilm structure (42).

2.9. Confocal Laser Scanning Microscopy for Biofilm Visualization

Pseudomonas aeruginosa KPW.1-S1 and HRW.1-S3 biofilm formation was further studied using confocal laser scanning microscopy (CLSM) to evaluate the impact of LCLE-Ag NPs. Biofilms were grown on coverslips in 24-well plates and incubated at 37 °C (150 rpm). Following 24 hours of incubation, the coverslips were carefully washed twice with PBS and stained with 0.005% (w/v) acridine orange for 5 minutes. Following staining, the coverslips were rinsed twice with PBS and mounted onto clean glass slides using 5% glycerol. Transparent nail polish was used to seal the edges of the coverslip. The samples were examined using a Nikon confocal microscope with an excitation wavelength of 488 nm, and emission was detected in the 293–586 nm range (42).

2.10. Biofilm eradication assay

Similarly, a pre-formed biofilm load assay was performed on *Pseudomonas aeruginosa* KPW.1-S1 and HRW.1-S3, to estimate the biofilm eradication potential of the LCLE-Ag NPs on the formed biofilm. The biofilm was first grown for 24 hours. After this initial growth period of 24 hours, the media with planktonic cells were carefully removed and replaced with fresh BH 2% glucose media with different concentrations of LCLE-Ag NPs. The rest of the steps were followed according to the biofilm load assay protocol.

2.11. Cell Viability Assay

The cytotoxicity of LCLE-Ag NPs, along with their control (equivalent Ag concentration), was tested on HEK293T cells using a standardized 3-(4,5-dimethylthiazol-2-yl)-2,5-diphenyltetrazolium bromide (MTT) colorimetric assay protocol (35). Briefly, human epithelial kidney like (HEK293T) cells were seeded in a 96-well culture plate with 5000 cells/well and allowed to adhere overnight under standard conditions (37 °C, 5% CO_2). Cells were then treated with 10- 20- 50- 100 μg/mL LCLE-Ag NPs and their respective silver concentrations, along with an untreated control, for 24 hours. Following 24-hour treatment, the MTT assay was performed by replacing spent media with fresh medium containing 0.5 mg/mL of MTT solution (SRL, India). After 4-hour incubation in darkness at (37 °C, 5% CO_2), the formazan conversion reaction was terminated by carefully removing the MTT solution and dissolving the crystalline products with 100 μL dimethyl sulfoxide per well and then incubated for 30 minutes in the dark at 37 °C. Then, the absorbance was taken in a microplate reader at 595 nm. The cytotoxic effect of the LCLE-Ag NPs and $AgNO_3$ was expressed as cell viability percentage compared to the untreated control.

2.12. Statistical analysis

The statistical analysis was carried out using GraphPad Prism 9.5.1, with results expressed as mean ± standard error. A two-tailed Student's t-test was employed to evaluate differences between group means, with statistically significant differences denoted by asterisks (*P<0.05; **P<0.01; ***P<0.001).

3. Results

3.1. Characterization of green synthesized silver nanoparticles

3.1.1. UV-Visible spectral analysis

UV-Visible spectroscopy was performed to check the absorbance band of the prepared LCLE-Ag NP. The distinct peak between 300-500 nm of the prepared nanoparticles revealed the Surface Plasmon Resonance (SPR) peak, indicating the formation of the nanoparticle, with the maximum absorbance at 416 nm (Figure 1).

3.1.2. Dynamic Light Scattering analysis

Dynamic Light Scattering was studied to examine the average size and PDI of LCLE-Ag NPs. The average size of the nanoparticles determined by the size analyzer was 35 nm (Figure 2a). The synthesized nanoparticles showed a PDI of 0.3, signifying a homogenous population of nanoparticles. Overall, the result suggests that the synthesized nanoparticle is homogeneous, with a size of around 20-40 nm.

3.1.3. Zeta potential analysis

The surface charge of the synthesized LCLE-Ag NPs was determined using a zeta sizer. The graph displays the corresponding average zeta potential of -9.53 mV (Figure 2b). This zeta potential value implies the stability of the synthesized nanoparticles, as the negatively charged nanoparticles will exhibit a repulsive force, resulting in enhanced stability.

3.1.4. SEM and EDX analysis

Scanning Electron Microscopy was performed to depict the morphology of the synthesized nanoparticles (Figure 3a). The morphology of the prepared nanoparticles was observed to be nearly spherical with fair agglomeration. The topographical analysis revealed that the average particle size is 26 nm.

Energy Dispersive X-ray Spectroscopy (EDX) analysis was used to analyze the elemental composition of the synthesized LCLE-Ag NPs (Supplementary Figure S1a). The graph indicates a significant peak for Silver with a weight percentage of nearly 70%. The EDX analysis also confirmed the formation of LCLE-Ag NPs.

The EDX of *L. camara* leaf extract was done to analyze elemental composition (Supplementary Figure S1 b). Quantitative analysis elucidates that Cl, O, Ca, K, Si, and Ag elements are present in the leaf extract. Out of these, O and K carried out the majority weight percentages of 78.53% and 11.26%, respectively, with traces of other elements.

3.1.5. Transmission Electron Microscopy

The Transmission Electron Microscopy images indicated the formation of approximately spherical nanoparticles with slight agglomeration (Figure 3b).

3.1.6. AFM analysis

AFM observations corroborate the obtained morphological results of synthesized nanoparticles. The AFM images revealed that LCLE-Ag NPs exhibited a nearly spherical shape with some degree of agglomeration from lateral and horizontal views (Figure 3c, 3d). The height and latitude studied in the analysis support the data, suggesting the spherical shape of the prepared nanoparticle.

3.1.7. ATR-Fourier Transform Infrared (FTIR) spectroscopy

ATIR-FTIR Fourier Transform Infrared (FTIR) spectroscopy was conducted to identify functional groups in *L. camara* leaf extract as well as in the synthesized LCLE-Ag NPs. The major intense peaks in the leaf extract were observed approximately around 1000 cm^{-1}, 1200 cm^{-1}, 1700 cm^{-1}, 2900 cm^{-1} and 3000 cm^{-1}. The firm, intense broad bands at 2921.62 cm^{-1} and 2853.67 cm^{-1} suggest the presence of amine salts and alkane groups in LCLE-Ag NPs, respectively (Figure 4a). The small peak around 2500 cm^{-1} is the characteristic peak of the nitrile group and alkyne in the nanoparticles. Another intense band between 1500 cm^{-1}-1750 cm^{-1} is attributed to a carbonyl group (41). The peak signifying carbonyl group was found to be weaker in synthesized LCLE-Ag NPs when compared with *L. camara* leaf extract (Figure 4b). This difference suggests participation of the carbonyl groups present in the *L. camara* leaf extract along with the silver during the nanoparticle formation. The phenol groups present in the leaf extract, around 1300 cm^{-1}, are likely to be responsible for the bio-reduction of silver ions (45). The medium stretching of alkane and aldehyde, along with minor stretching of nitrile group and alcohols or ethers, indicates the presence of different phytoconstituents of *L. camara* in the nanoparticles, confirming the green synthesis.

3.2. Antibacterial effect of LCLE-Ag NPs against *Pseudomonas aeruginosa*

The minimum inhibitory concentration of prepared LCLE-Ag Np was checked at 5-10-20-50-100 μg/mL concentrations against *Pseudomonas aeruginosa* KPW.1-S1 and HRW.1-S3 (Figure 5a). For KPW.1-S1, at lower concentrations (5 μg/mL and 10 μg/mL), the nanoparticles exhibited non-

significant effects, with only slight reductions in bacterial growth. At 20 μg/mL, the nanoparticles achieved a significant reduction of 0.25-fold. However, 50 μg/mL concentration of nanoparticles resulted in a significant decrease of 0.996-fold. In the presence of 100 μg/mL, bacterial growth was entirely inhibited, confirming the effectiveness of LCLE-Ag NPs at this dose.

Similarly, when the minimum inhibitory concentration assay was performed on *Pseudomonas aeruginosa* HRW.1-S3 (Figure 5b), at the lower doses of nanoparticles (5- 10- 20 μg/mL), the LCLE-Ag NPs showed a 0.27-fold, 0.32-fold, and 0.44-fold effect on bacterial growth, respectively. At the 50 μg/mL LCLE-Ag NPs, the bacterial growth was significantly reduced by 0.85-fold. At 100 μg/mL LCLE-Ag NPs, the bacterial growth was inhibited entirely, confirming the efficacy of LCLE-Ag NPs at this dose.

Therefore, the MIC concentration of the LCLE-Ag NPs for both the strains was determined to be 100 μg/mL.

3.3. Effect of LCLE-Ag NPs on Biofilm Formation of *Pseudomonas aeruginosa*

The Biofilm load assay was performed to study the effectiveness of the prepared LCLE-Ag NPs against *Pseudomonas aeruginosa* KPW.1-S1 and HRW.1-S3 biofilm. Interestingly, for KPW.1-S1, it was observed that when LCLE was used at a concentration of 1.33mg/mL (which was used during nanoparticle preparation), it encouraged biofilm formation significantly by a 4.85-fold compared to the untreated control (Figure 6a). Importantly, it was observed that the prepared nanoparticles could reduce the biofilm with increasing doses. In the presence of 10 μg/mL LCLE-Ag NP, a non-significant decrease was seen but at 20 μg/mL concentration of LCLE-Ag NPs, the biofilm load decreased by 0.75-fold compared to the control. Higher concentration (50 μg/mL) of LCLE-Ag NP further reduced the biofilm by 0.67-fold and at the concentration of 100 μg/mL, further reduction in biofilm formation was observed, with a 0.97-fold decrease relative to the control (Figure 6a).

The biofilm load assay was also performed against *Pseudomonas aeruginosa* HRW.1-S3 (Figure 6b). Relative to control, the 1.33 mg/mL *L. camara* leaf extract showed a significant 4.73-fold increase in biofilm load. At the lower doses of 10 μg/mL and 20 μg/mL, the nanoparticles had a

non-significant effect on the biofilm, but at higher doses of 50 µg/mL and 100 µg/mL, the biofilm load was significantly decreased to 0.65-fold and 0.73-fold, respectively (Figure 6b).

The images of the crystal violet-stained biofilms are given in Supplementary Figure S2 as a supporting document.

3.4. Effect of LCLE-Ag NPs on the architecture of *Pseudomonas aeruginosa* biofilms

To visualize the reduction in the biofilm load and alterations in biofilm structures in the presence of LCLE-Ag NPs, scanning electron microscopy (SEM) and confocal laser scanning microscopy (CLSM) were performed.

3.4.1. SEM analysis

The SEM was performed to study the structure of the PA biofilms. For KPW.1-S1 (Figure 7a), it was observed that most of the cells in control samples adhered to the surface and with each other to form a dense biofilm. Treatment with 1.33 mg/mL *L. camara* leaf extract induced the bacterial cells to form a thick and robust biofilm with increased presence of extracellular polymeric substances and increased number of canopies. However, with the introduction of increasing concentrations of prepared nanoparticles, it was observed that the biofilm thickness decreased significantly. In the presence of 50 µg/mL of nanoparticles, mostly individually scattered cells were present with no substantial EPS production, whereas in the presence of 100 µg/mL of nanoparticles, very few individual cells, along with some cell debris, were visible (Figure 7a).

In the case of HRW.1-S3 (Figure 7b), the control condition showed the formation of a thick biofilm. The presence of LCLE alone further increased the biofilm formation, with a more thickened biofilm structure with an increased number of canopies. The introduction of low doses of nanoparticles decreased the overall biofilm formation in comparison to the control and LCLE alone. The presence of 50 µg/mL showed a few clumped cells, and in the highest dose (100 µg/mL), very few cells, along with cell debris, were visible (Figure 7b).

3.4.2. CLSM analysis

Like SEM, CLSM analysis also showed the inhibitory effect of LCLE-Ag NPs on biofilm formation by PA strains (Figure 8). In comparison to the control samples, thick biofilm formation was observed in the presence of 1.33 mg/mL *L. camara* leaf extract. The biofilm formation was found to be decreased with the increasing concentrations of prepared LCLE-Ag NPs for both of the PA strains (Figure 8a,b).

3.5. Effect of LCLE-Ag NPs on the preformed biofilm of *Pseudomonas aeruginosa*

Biofilm eradication assays were performed against *Pseudomonas aeruginosa* KPW.1-S1 and HRW.1-S3 to study the effectiveness of LCLE-Ag NPs on the preformed biofilm. For preformed biofilm in KPW.1-S1, addition of LCLE further increased the biofilm by 5.41-fold, whereas the LCLE-Ag NPs showed a decrease in the formed biofilm. Although there was no significant decrease in the presence of lower doses (10 µg/mL and 20 µg/mL) of nanoparticle, higher doses of nanoparticles, (50 µg/mL and 100 µg/mL) could reduced the formed biofilm by 0.71-fold and 0.82-fold, respectively, showcasing its ability to eradicate biofilm (Figure 9a).

In the case of HRW.1-S3, the 1.33 mg/ml LCLE showed a 5.62-fold increase in biofilm load. The lower doses of nanoparticles (10 µg/mL and 20 µg/mL) resulted in a non-significant decrease in the formed biofilm, whereas the higher doses of nanoparticles (50 µg/mL and 100 µg/mL) reduced the formed biofilm significantly by 0.61-fold and 0.67-fold (Figure 9b).

The images of the crystal violet-stained biofilm are given in Supplementary Figure S3 as a supporting document.

3.6. Effect of LCLE-Ag NPs on the viability of HEK293T cells

The cytotoxic effect of different doses of LCLE-Ag NPs and their equivalent doses of silver ions was studied in HEK293T cells. For all the doses, LCLE-Ag NPs could not induce any significant cytotoxicity in HEK293T cells as compared to the untreated cells (Figure 10). Whereas the equivalent doses of silver showed significant cytotoxicity in the HEK293T cells. These results clearly indicate that normal silver ions are toxic to cells, but the green synthesized LCLE-Ag NP

has no significant toxicity on the HEK293T cells, making it as a potent candidate for medicinal uses.

4. Discussion

We were able to green synthesize the silver nanoparticles using *L. camara* leaf extract, which has emerged as an eco-friendly and sustainable approach. It holds the phytochemical constituents of the plant extract to reduce silver ions Ag^+ to Ag^0 and stabilize the nanoparticles by acting as a capping agent. This method provides a cost-effective, adaptable alternative for nanoparticle synthesis (32,41).

UV-visible spectroscopy serves as a key analytical tool for determining the formation and assessing the stability of metal nanoparticles in aqueous solution with a distinct spectrum. The yellowish-brown colour indicates the formation of LCLE-Ag NPs due to surface plasmon resonance (SPR). It was confirmed through UV-vis spectroscopy, with the SPR peak observed between 350-470 nm, indicating nanoparticle synthesis (46). The zeta potential and DLS concluded the stability with values indicating strong electrostatic repulsion and a size range of 30-50 nm of the nanoparticles (47). The phytochemicals present in the leaf extract may have played a key role in enhancing the repulsion between negatively charged particles. This capping of the silver particles effectively prevented agglomeration, resulting in enhanced stability of the nanoparticles (41). The DLS analysis showed a PDI value of 0.3, which signifies a homogeneous size distribution of the LCLE-Ag NPs. The average value of zeta potential was -9.54, which could be due to leaf extract phytoconstituents (19).

The SEM analysis of LCLE-Ag NPs revealed the size of nanoparticles to be 25-35 nm, having a spherical morphology, which was further confirmed by TEM and AFM analysis. The TEM analysis revealed the size to be spherical and slight agglomeration, while AFM images revealed the same. This clustering is normal due to some factors, such as concentration and environmental conditions, despite their stabilizing effects (48,49). The EDX analysis confirmed the elemental composition of the synthesized LCLE-Ag NPs. The EDX spectrum for *L. camara* leaf extract suggests a weight percentage of 0% for Ag, indicating that the amount of silver in nanoparticles is not from *L. camara* but due to the successful formation of nanoparticles. The ATIR-FTIR study

on chemical composition further confirms the presence of several functional groups and suggests their involvement in the formation of nanoparticles. The spectra showed a strong signal for phytoconstituents, employing the successful formation of green synthesized silver nanoparticles. The FTIR spectra revealed prominent peaks corresponding to hydroxyl (-OH), carbonyl (C=O), and amine (N-H) groups, which are indicative of the phytochemical constituents from *L. camara* acting as reducing and stabilizing agents. These functional groups likely facilitate the capping of nanoparticles, enhancing their stability and bioactivity (31,50).

Additionally, we were able to show significant antibacterial and antibiofilm potential as well as biofilm eradicating ability of the prepared LCLE-Ag NP against *Pseudomonas aeruginosa* KPW.1-S1 and HRW.1-S3. In the MIC assay, both strains of PA demonstrated significant antibacterial activity. The higher concentration of LCLE-Ag NPs significantly reduced the bacterial growth. The probable reason for this antibacterial activity can be attributed to the disruption of the cell membranes, ROS generation, and impact on overall cell functions (51,52). The biofilm load assay of both strains showed that the synthesized nanoparticle had an inhibitory effect on the biofilm load in a dose-dependent manner. At higher concentrations of LCLE-Ag NPs, the biofilm load of both strains has been reduced significantly. The nanoparticles were also able to abolish the formed biofilm for both strains. We further investigated the topology and morphological details of the KPW.1-S1 and HRW.1-S3 biofilm in detail.

CLSM and SEM further investigated the biofilm morphology. The morphological study by SEM and CLSM on the biofilm supported the biofilm load analysis. SEM data revealed a significant reduction in biofilm biomass and reduced EPS in nanoparticle-treated samples in both strains of PA. CLSM images clearly showed decreased overall biofilm formation in the presence of nanoparticles. Having addressed the bactericidal and anti-biofilm properties of LCLE-Ag NPs, it was essential to assess the toxicity of LCLE-Ag NP on the mammalian cell line. The MTT assay of Human Kidney Epithelial-like cells with different doses of LCLE-Ag NPs exhibited minimal toxicity, with cell viability ranging from 90% to 100%. In contrast, equivalent doses of silver in LCLE-Ag NP alone showed high toxicity even in the lowest treatment dose. These findings highlighted the efficiency of the LCLE-Ag NPs compared to silver.

Several studies have demonstrated the successful green-synthesis of silver nanoparticles and their efficacy against PA (53,54). Ajitha et al. reported the antibacterial potential of *L. camara* leaf,

which exhibited positive effects against both Gram-negative bacteria and Gram-positive bacteria (55). In another study, Momani et al. proved the antibiofilm activity of biosynthesized silver nanoparticles using *P. harmala* seed extract against PA isolates obtained from cystic fibrosis patients, highlighting the potential of plant-mediated nanoparticles and encouraging exploration of *L. camara* leaf extract as a biocompatible agent (22). Our present work further advances this line of research by showing that *L. camara*-mediated silver nanoparticles are capable of exerting antibacterial effect and antibiofilm effects at the level of both formation and eradication against *Pseudomonas aeruginosa.* Additionally, *L. camara*-mediated silver nanoparticles could not exert any significant cytotoxicity assay against Human Kidney Epithelial-like cells.

The enhanced efficacy and reduced toxicity of LCLE-Ag NPs synthesized using *L. camara* may be attributed to their nanoscale size, high surface area-to-volume ratio, and potential synergistic effects of bioactive phytochemicals present in the extract. Future studies on elucidating the molecular mechanism underlying the antibiofilm activity of the LCLE-AgNPs will help to find relevant targets in Pseudomonas biofilms for the remedial purposes.

5. Conclusion

The present study explored the efficacy of these biosynthesized LCLE-Ag NPs against the pathogenic bacterium *Pseudomonas aeruginosa* KPW.1-S1, focusing on both antibacterial and antibiofilm activities. Phytochemicals in the plant extract, such as flavonoids, tannins, and phenolic compounds, likely played a dual role as reducing and capping agents, ensuring nanoparticle formation and stability. The studied characterization of the LCLE-Ag NP met the standard nanoparticle values with respect to its size, shape, morphology, and functional surface groups, enhancing their biological activity. These nanoparticles exhibited significant antibacterial and antibiofilm potential. While it was tested on a mammalian cell line, it showed no cytotoxic effect.

In conclusion, the green synthesis of silver nanoparticles using *L. camara* leaf offers an environmentally sustainable approach with significant antibacterial and antibiofilm potential against *Pseudomonas aeruginosa* KPW.1-S1 and HRW.1-S3. These findings pave the way for developing novel nanomaterials for combating multidrug-resistant pathogens without causing any damage to mammalian cells.

Acknowledgment

All authors would like to acknowledge the imaging facilities of the Indian Institute of Science Education and Research, Kolkata. The authors would also acknowledge Prof. Rahul Banerjee, DCS IISER Kolkata, for helping with the ATR-FTIR analysis. Authors also thank Arundhaty Pal and Sourav Sanyal, DBS IISER Kolkata for helping in MTT assays. SKS acknowledges IISER Kolkata for providing fellowship.

CRediT authorship contribution statement

ADR and SKS: Conceptualization, Methodology, Investigation, Formal analysis, Data curation, Writing of the manuscript. **Tapas Kumar Sengupta**: Conceptualization, analysis, review & editing of the manuscript.

Funding

The study was funded by the Indian Institute of Science Education and Research, Kolkata. The funding source has no involvement in the study design; collection, analysis and interpretation of data and writing and preparation of the article.

Declaration of competing interest

The authors declare that they have no known competing financial interests or personal relationships that could have appeared to influence the work reported in this paper.

Data availability

All data generated or analyzed during this study are included in this present article.

Declaration

Conflict of interest

The authors declare that there is no conflict of interest.

Ethical Approval

Not applicable.

Consent to Participate

All authors had consented to participate in the study.

Consent for Publication

All authors have given consent for publication.

References

1. Mirzaei R, Mohammadzadeh R, Alikhani MY, Shokri Moghadam M, Karampoor S, Kazemi S, et al. The biofilm-associated bacterial infections unrelated to indwelling devices. IUBMB Life [Internet]. 2020;72(7):1271–85. Available from: https://iubmb.onlinelibrary.wiley.com/doi/abs/10.1002/iub.2266
2. Pressler T, Bohmova C, Conway S, Dumcius S, Hjelte L, Høiby N, et al. Chronic Pseudomonas aeruginosa infection definition: EuroCareCF Working Group report. J Cyst Fibros. 2011;10 Suppl 2:S75-8.
3. Gondil VS, Subhadra B. Biofilms and their role on diseases. BMC Microbiol [Internet]. 2023;23(1):203. Available from: https://doi.org/10.1186/s12866-023-02954-2
4. Vestby LK, Grønseth T, Simm R, Nesse LL. Bacterial Biofilm and its Role in the Pathogenesis of Disease. Antibiotics [Internet]. 2020;9(2):59. Available from: https://www.mdpi.com/2079-6382/9/2/59
5. Ferris RA, McCue PM, Borlee GI, Glapa KE, Martin KH, Mangalea MR, et al. Model of Chronic Equine Endometritis Involving a Pseudomonas aeruginosa Biofilm. Infect Immun [Internet]. 2017;85(12):10.1128/iai.00332-17. Available from: https://journals.asm.org/doi/abs/10.1128/iai.00332-17
6. Tuon FF, Dantas LR, Suss PH, Tasca Ribeiro VS. Pathogenesis of the Pseudomonas aeruginosa Biofilm: A Review. Pathogens. 20220227th ed. 2022;11(3).
7. Potera C. Forging a link between biofilms and disease. Science (1979). 1999;283(5409):1837, 1839.
8. Thi MTT, Wibowo D, Rehm BHA. Pseudomonas aeruginosa Biofilms. Int J Mol Sci [Internet]. 2020;21(22):8671. Available from: https://www.mdpi.com/1422-0067/21/22/8671
9. Sharma D, Misba L, Khan AU. Antibiotics versus biofilm: an emerging battleground in microbial communities. Antimicrob Resist Infect Control. 20190516th ed. 2019;8:76.
10. Tabassum N, Khan F, Jeong GJ, Jo DM, Kim YM. Silver nanoparticles synthesized from Pseudomonas aeruginosa pyoverdine: Antibiofilm and antivirulence agents. Biofilm [Internet]. 2024;7:100192. Available from: https://www.sciencedirect.com/science/article/pii/S2590207524000170
11. Parrino B, Schillaci D, Carnevale I, Giovannetti E, Diana P, Cirrincione G, et al. Synthetic small molecules as anti-biofilm agents in the struggle against antibiotic resistance. Eur J Med Chem. 20181017th ed. 2019;161:154–78.
12. de la Fuente-Núñez C, Reffuveille F, Haney EF, Straus SK, Hancock RE. Broad-spectrum anti-biofilm peptide that targets a cellular stress response. PLoS Pathog. 20140522nd ed. 2014;10(5):e1004152.
13. Kaplan JB. Biofilm Matrix-Degrading Enzymes. In: Donelli G, editor. Microbial Biofilms: Methods and Protocols [Internet]. New York, NY: Springer New York; 2014. p. 203–13. Available from: https://doi.org/10.1007/978-1-4939-0467-9_14

14. Furfaro LL, Payne MS, Chang BJ. Bacteriophage Therapy: Clinical Trials and Regulatory Hurdles. Front Cell Infect Microbiol. 20181023rd ed. 2018;8:376.
15. Hegde S, Nilyanimit P, Kozlova E, Anderson ER, Narra HP, Sahni SK, et al. CRISPR/Cas9-mediated gene deletion of the ompA gene in symbiotic Cedecea neteri impairs biofilm formation and reduces gut colonization of Aedes aegypti mosquitoes. PLoS Negl Trop Dis. 20191202nd ed. 2019;13(12):e0007883.
16. Carpenter BL, Situ X, Scholle F, Bartelmess J, Weare WW, Ghiladi RA. Antiviral, Antifungal and Antibacterial Activities of a BODIPY-Based Photosensitizer. Molecules [Internet]. 2015;20(6):10604–21. Available from: https://www.mdpi.com/1420-3049/20/6/10604
17. Koo H, Allan RN, Howlin RP, Stoodley P, Hall-Stoodley L. Targeting microbial biofilms: current and prospective therapeutic strategies. Nat Rev Microbiol. 20170925th ed. 2017;15(12):740–55.
18. Huang D ni, Wang J, Ren K feng, Ji J. Functionalized biomaterials to combat biofilms. Biomater Sci [Internet]. 2020;8(15):4052–66. Available from: http://dx.doi.org/10.1039/D0BM00526F
19. Öztürk K, Kaplan M, Çalış S. Effects of nanoparticle size, shape, and zeta potential on drug delivery. Int J Pharm [Internet]. 2024;666:124799. Available from: https://www.sciencedirect.com/science/article/pii/S0378517324010330
20. Klębowski B, Depciuch J, Parlińska-Wojtan M, Baran J. Applications of Noble Metal-Based Nanoparticles in Medicine. Int J Mol Sci. 20181213th ed. 2018;19(12).
21. Ying S, Guan Z, Ofoegbu PC, Clubb P, Rico C, He F, et al. Green synthesis of nanoparticles: Current developments and limitations. Environ Technol Innov [Internet]. 2022;26:102336. Available from: https://www.sciencedirect.com/science/article/pii/S2352186422000359
22. Al-Momani H, Almasri M, Al Balawi D, Hamed S, Albiss BA, Aldabaibeh N, et al. The efficacy of biosynthesized silver nanoparticles against Pseudomonas aeruginosa isolates from cystic fibrosis patients. Sci Rep. 20230601st ed. 2023;13(1):8876.
23. Han C, Romero N, Fischer S, Dookran J, Berger A, Doiron AL. Recent developments in the use of nanoparticles for treatment of biofilms. Nanotechnol Rev [Internet]. 2017;6(5):383–404. Available from: https://doi.org/10.1515/ntrev-2016-0054
24. Ali SG, Jalal M, Ahmad H, Sharma D, Ahmad A, Umar K, et al. Green Synthesis of Silver Nanoparticles from Camellia sinensis and Its Antimicrobial and Antibiofilm Effect against Clinical Isolates. Materials [Internet]. 2022;15(19):6978. Available from: https://www.mdpi.com/1996-1944/15/19/6978
25. Khedr WE, Shaheen MNF, Elmahdy EM, El-Bendary MA, Hamed AA, Mohamedin AH. Silver and gold nanoparticles: Eco-friendly synthesis, antibiofilm, antiviral, and anticancer bioactivities. Prep Biochem Biotechnol. 20230823rd ed. 2024;54(4):470–82.
26. Wypij M, Jędrzejewski T, Trzcińska-Wencel J, Ostrowski M, Rai M, Golińska P. Green Synthesized Silver Nanoparticles: Antibacterial and Anticancer Activities,

Biocompatibility, and Analyses of Surface-Attached Proteins. Front Microbiol. 20210422nd ed. 2021;12:632505.

27. Ansari MA, Khan HM, Khan AA, Cameotra SS, Pal R. Antibiofilm efficacy of silver nanoparticles against biofilm of extended spectrum β-lactamase isolates of Escherichia coli and Klebsiella pneumoniae. Appl Nanosci [Internet]. 2014;4(7):859–68. Available from: https://doi.org/10.1007/s13204-013-0266-1

28. Salomoni R, Léo P, Montemor AF, Rinaldi BG, Rodrigues M. Antibacterial effect of silver nanoparticles in Pseudomonas aeruginosa. Nanotechnol Sci Appl. 20170629th ed. 2017;10:115–21.

29. Augustine R, Hasan A, Primavera R, Wilson RJ, Thakor AS, Kevadiya BD. Cellular uptake and retention of nanoparticles: Insights on particle properties and interaction with cellular components. Mater Today Commun [Internet]. 2020;25:101692. Available from: https://www.sciencedirect.com/science/article/pii/S2352492820327033

30. de la Fuente-Núñez C, Reffuveille F, Haney EF, Straus SK, Hancock RE. Broad-spectrum anti-biofilm peptide that targets a cellular stress response. PLoS Pathog. 20140522nd ed. 2014;10(5):e1004152.

31. Alomar TS, AlMasoud N, Awad MA, AlOmar RS, Merghani NM, El-Zaidy M, et al. Designing Green Synthesis-Based Silver Nanoparticles for Antimicrobial Theranostics and Cancer Invasion Prevention. Int J Nanomedicine. 20240521st ed. 2024;19:4451–64.

32. Barreto F, Sousa E, Campos A, Costa J, Rodrigues F. Antibacterial Activity of Lantana camara Linn and Lantana montevidensis Brig Extracts from Cariri-Ceará, Brazil. J Young Pharm. 2010;2(1):42–4.

33. Mansoori A, Singh NK, Dubey SK, Thakur TK, Alkan N, Das SN, et al. Phytochemical Characterization and Assessment of Crude Extracts From Lantana camara L. for Antioxidant and Antimicrobial Activity. In: Frontiers in Agronomy. 2020.

34. Vishal H, Firoj A, Asha S, Rohankumar C. Phytochemical analysis and antimicrobial activity of Lantana camara. International Journal of Pharmaceutical Chemistry and Analysis [Internet]. 2022;2022:15736. Available from: https://www.ijpca.org/article-details/15736

35. Pal A, Sanyal S, Das S, Sengupta TK. Effect of Lantana camara Ethanolic Leaf Extract on Survival and Migration of MDA-MB-231 Triple-Negative Breast Cancer Cell Line. J Herb Med [Internet]. 2024;43:100837. Available from: https://www.sciencedirect.com/science/article/pii/S2210803323002154

36. Bruna T, Maldonado-Bravo F, Jara P, Caro N. Silver Nanoparticles and Their Antibacterial Applications. Int J Mol Sci. 20210704th ed. 2021;22(13).

37. Sakthi Devi R, Girigoswami A, Siddharth M, Girigoswami K. Applications of Gold and Silver Nanoparticles in Theranostics. Appl Biochem Biotechnol. 20220513th ed. 2022;194(9):4187–219.

38. Yadav S, Pawar S, Patil S. Inhibition of Pseudomonas aeruginosa Biofilm Formation Using Silver Nanoparticles. Cureus. 20250122nd ed. 2025;17(1):e77848.

39. Omran BA, Tseng BS, Baek KH. Nanocomposites against Pseudomonas aeruginosa biofilms: Recent advances, challenges, and future prospects. Microbiol Res [Internet]. 2024;282:127656. Available from: https://www.sciencedirect.com/science/article/pii/S0944501324000570
40. Abdel-Fatah SS, Mohammad NH, Elshimy R, Mosallam FM. Impeding microbial biofilm formation and Pseudomonas aeruginosa virulence genes using biologically synthesized silver Carthamus nanoparticles. Microb Cell Fact [Internet]. 2024;23(1):240. Available from: https://doi.org/10.1186/s12934-024-02508-9
41. Ajitha B, Ashok Kumar Reddy Y, Sreedhara Reddy P. Green synthesis and characterization of silver nanoparticles using Lantana camara leaf extract. Mater Sci Eng C Mater Biol Appl. 20150109th ed. 2015;49:373–81.
42. Kumar A, Saha SK, Banerjee P, Prasad K, Sengupta TK. Antibiotic-Induced Biofilm Formations in Pseudomonas aeruginosa Strains KPW.1-S1 and HRW.1-S3 are Associated with Increased Production of eDNA and Exoproteins, Increased ROS Generation, and Increased Cell Surface Hydrophobicity. Curr Microbiol. 20231117th ed. 2023;81(1):11.
43. Dasgupta D, Ghosh R, Sengupta TK. Biofilm-Mediated Enhanced Crude Oil Degradation by Newly Isolated Pseudomonas Species . ISRN Biotechnol. 2013 Mar 5;2013:1–13.
44. Bushnell LD, Haas HF. The Utilization of Certain Hydrocarbons by Microorganisms. J Bacteriol. 1941;41(5):653–73.
45. Manjamadha VP, Muthukumar K. Ultrasound assisted green synthesis of silver nanoparticles using weed plant. Bioprocess Biosyst Eng. 20160111th ed. 2016;39(3):401–11.
46. Kaur H, Kaur H, Sharma A. Study of SPR peak shifting of silver nanoparticles with change in surrounding medium. Mater Today Proc [Internet]. 2021;37:3574–6. Available from: https://www.sciencedirect.com/science/article/pii/S2214785320373090
47. Hoseini B, Jaafari MR, Golabpour A, Momtazi-Borojeni AA, Karimi M, Eslami S. Application of ensemble machine learning approach to assess the factors affecting size and polydispersity index of liposomal nanoparticles. Sci Rep [Internet]. 2023;13(1):18012. Available from: https://doi.org/10.1038/s41598-023-43689-4
48. Giri AK, Jena B, Biswal B, Pradhan AK, Arakha M, Acharya S, et al. Green synthesis and characterization of silver nanoparticles using Eugenia roxburghii DC. extract and activity against biofilm-producing bacteria. Sci Rep [Internet]. 2022;12(1):8383. Available from: https://doi.org/10.1038/s41598-022-12484-y
49. Jaast S, Grewal A. Green synthesis of silver nanoparticles, characterization and evaluation of their photocatalytic dye degradation activity. Current Research in Green and Sustainable Chemistry [Internet]. 2021;4:100195. Available from: https://www.sciencedirect.com/science/article/pii/S2666086521001429
50. Younis NS, Mohamed ME, El Semary NA. Green Synthesis of Silver Nanoparticles by the Cyanobacteria Synechocystis sp.: Characterization, Antimicrobial and Diabetic Wound-Healing Actions. Mar Drugs. 20220106th ed. 2022;20(1).

51. Zúñiga-Miranda J, Guerra J, Mueller A, Mayorga-Ramos A, Carrera-Pacheco SE, Barba-Ostria C, et al. Iron Oxide Nanoparticles: Green Synthesis and Their Antimicrobial Activity. Nanomaterials [Internet]. 2023;13(22):2919. Available from: https://www.mdpi.com/2079-4991/13/22/2919
52. Tiwari H, Samal K, Geed SR, Bera S, Das C, Mohanty K. Green synthesis of silver nanoparticles for ultrafiltration membrane surface modification and antimicrobial activity. Sustainable Chemistry for Climate Action [Internet]. 2023;3:100031. Available from: https://www.sciencedirect.com/science/article/pii/S2772826923000202
53. Kemala P, Idroes R, Khairan K, Ramli M, Ginting B, Helwani Z, et al. Eco-friendly synthesis of silver nanoparticles: Enhancing optimization reaction, characterization, and antimicrobial properties with Lantana camara from geothermal area. S Afr J Chem Eng [Internet]. 2025;51:57–67. Available from: https://www.sciencedirect.com/science/article/pii/S1026918524001306
54. Patil SP, Sahu KG, Andhale GS. Lantana camara mediated green synthesis of metallic nanoparticles: A mini review. Inorg Chem Commun [Internet]. 2024;160:111853. Available from: https://www.sciencedirect.com/science/article/pii/S138770032301465X
55. Ajitha B, Ashok Kumar Reddy Y, Shameer S, Rajesh KM, Suneetha Y, Sreedhara Reddy P. Lantana camara leaf extract mediated silver nanoparticles: Antibacterial, green catalyst. J Photochem Photobiol B [Internet]. 2015;149:84–92. Available from: https://www.sciencedirect.com/science/article/pii/S1011134415001839

Figure 1.

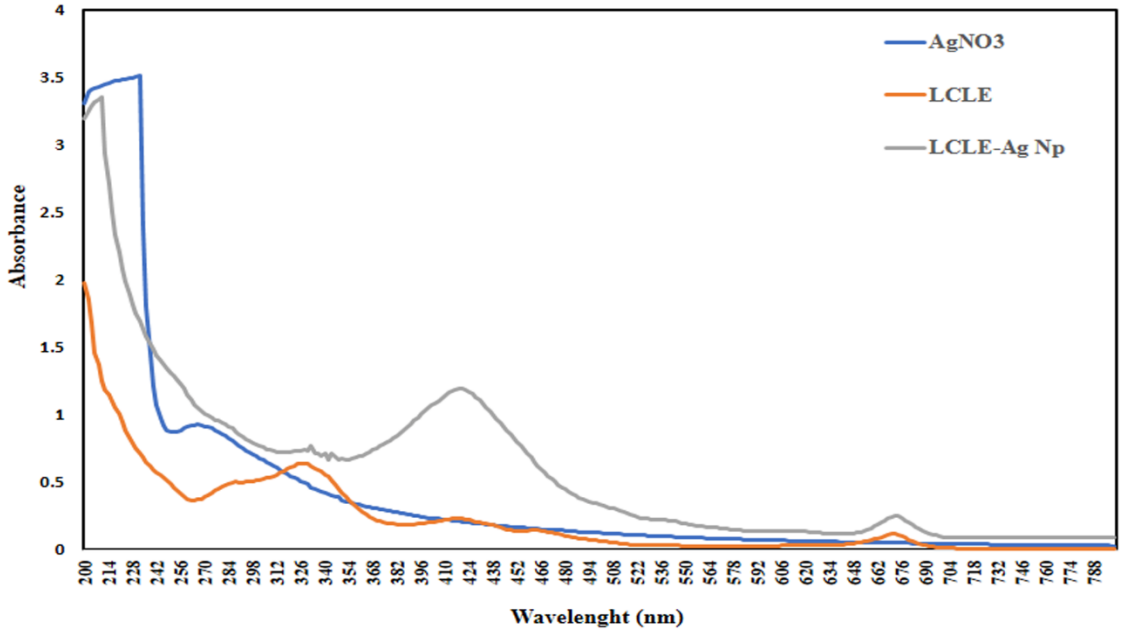

Fig. 1 UV–vis absorbance spectra of $AgNO_3$ solution (blue line) and *L. camara* leaf extract (Orange line), and LCLE-Ag NPs (grey line)

Figure 2.

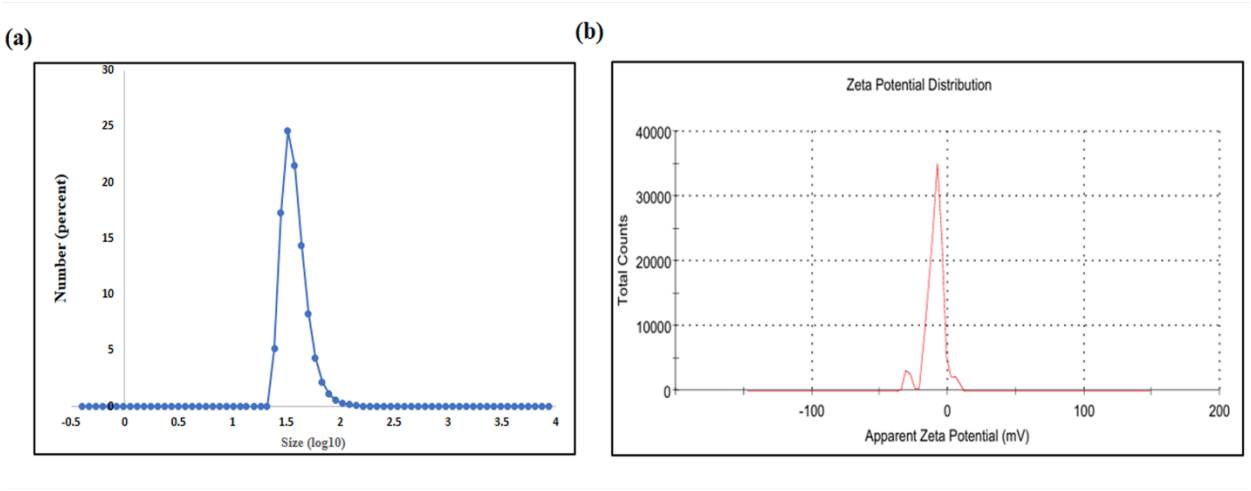

Fig. 2 Particle size and zeta potential analysis of green synthesized LCLE-Ag NPs (a) Particle size analysis, (b) Zeta potential analysis of LCLE-Ag NPs

Figure 3.

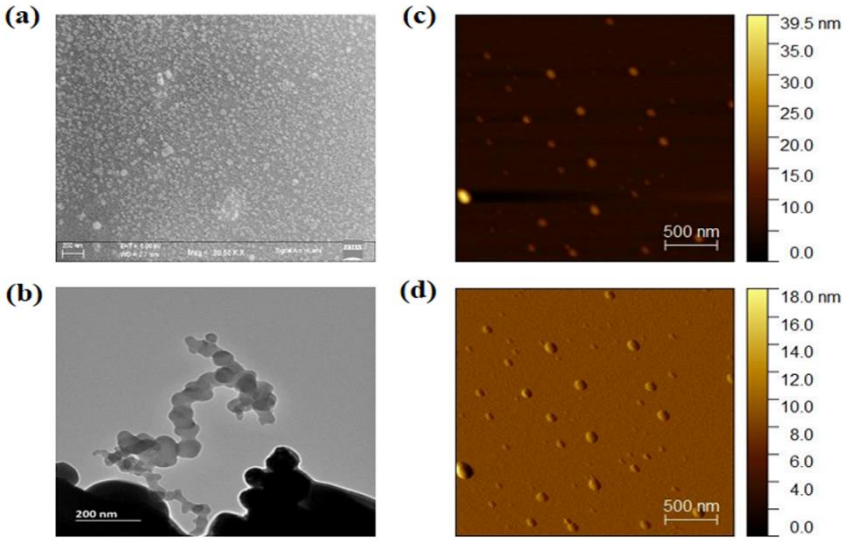

Fig. 3 Morphological and characteristic analysis of green synthesized LCLE-Ag NPs (a) SEM, (b) TEM, (c) AFM height, (d) AFM amplitude

Figure 4

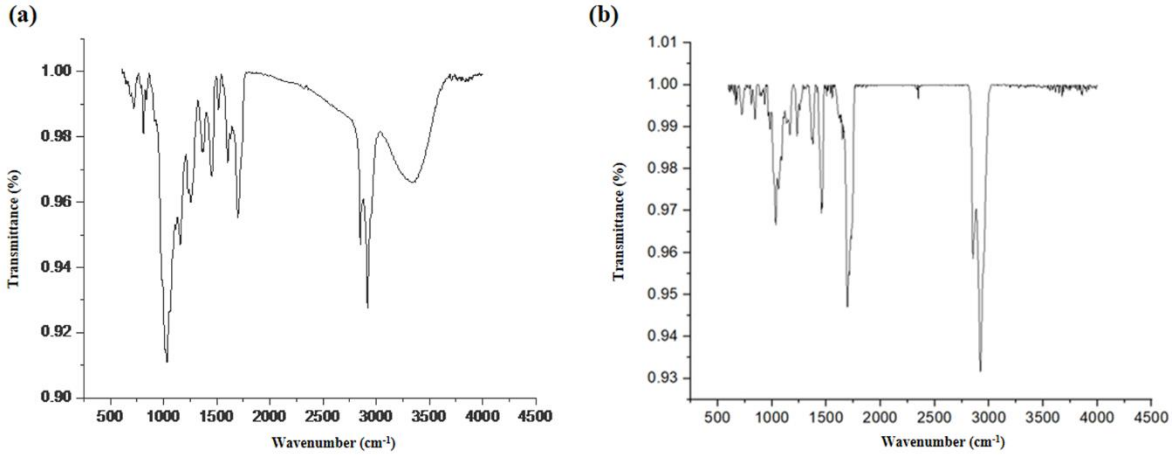

Fig. 4 FTIR spectrum of (a*) Lantana camara* leaf extract, (b) Green synthesized LCLE-Ag NPs

Figure 5.

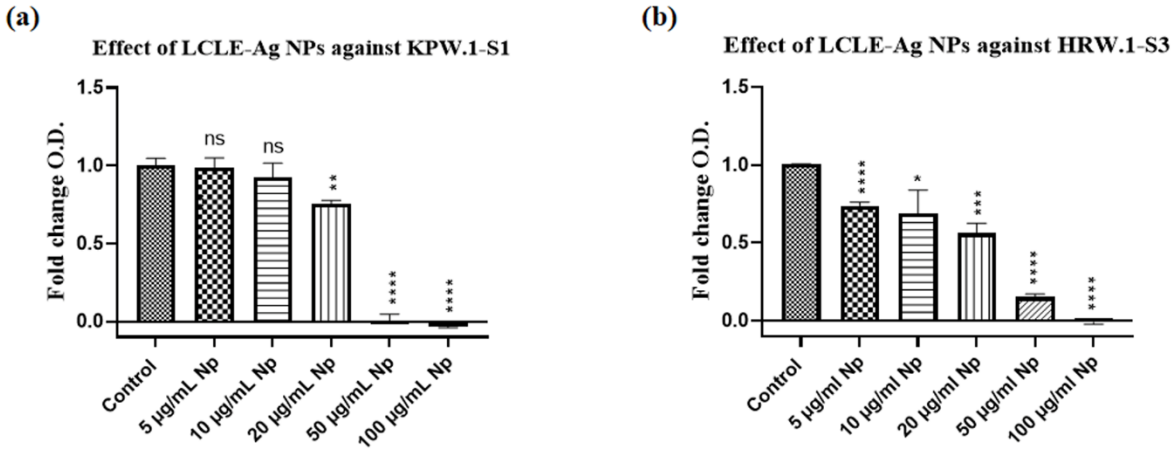

Fig. 5 Minimum inhibitory concentration assay of green synthesized LCLE-Ag NPs against *P. aeruginosa* (a) KPW.1-S1 and (b) HRW.1-S3; Data presented as the mean ± SEM; n=9; N=3; *, $P \leq 0.05$, **$P \leq 0.01$, ***$P \leq 0.001$, ****$P \leq 0.0001$, while 'ns' indicates non-significance

Figure 6.

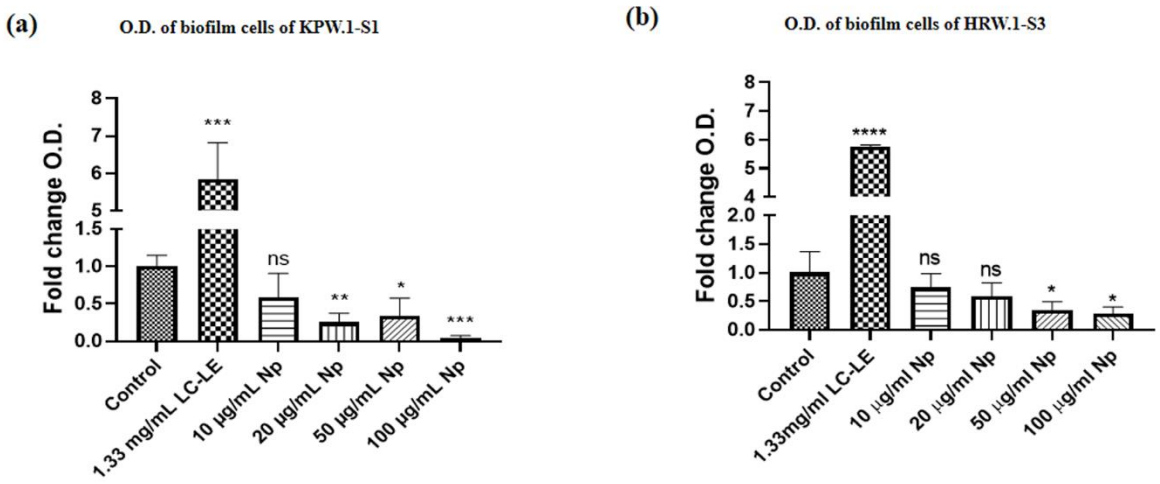

Fig. 6 Biofilm load assay of *P. aeruginosa* KPW.1-S1 and HRW.1-S3 in the presence of LCLE-Ag NP. (a) O.D. of biofilm cells of KPW.1-S1 (b) O.D. of biofilm cells of HRW.1-S3; Data represent mean ± SEM of n=9; N=3; *, $P \leq 0.05$, **$P \leq 0.01$, ***$P \leq 0.001$, ****$P \leq 0.0001$, while 'ns' indicates non-significance

Figure 7

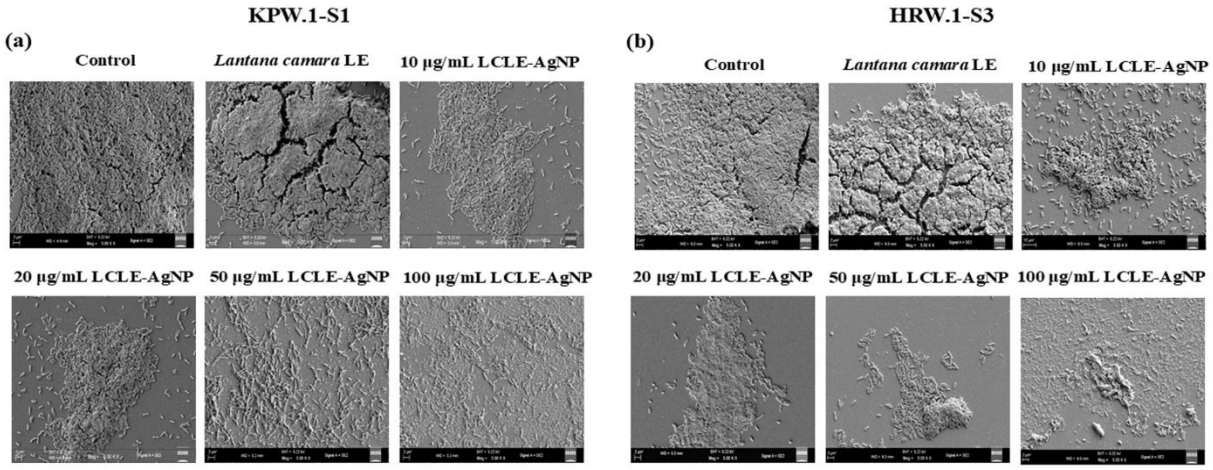

Fig. 7 Representative Scanning Electron Microscope images of *P. aeruginosa* biofilm in the presence of LCLE-Ag NP. (a) 5.0KX images of KPW.1-S1 biofilm (b) 5.0KX images of HRW.1-S3 biofilm

Figure 8

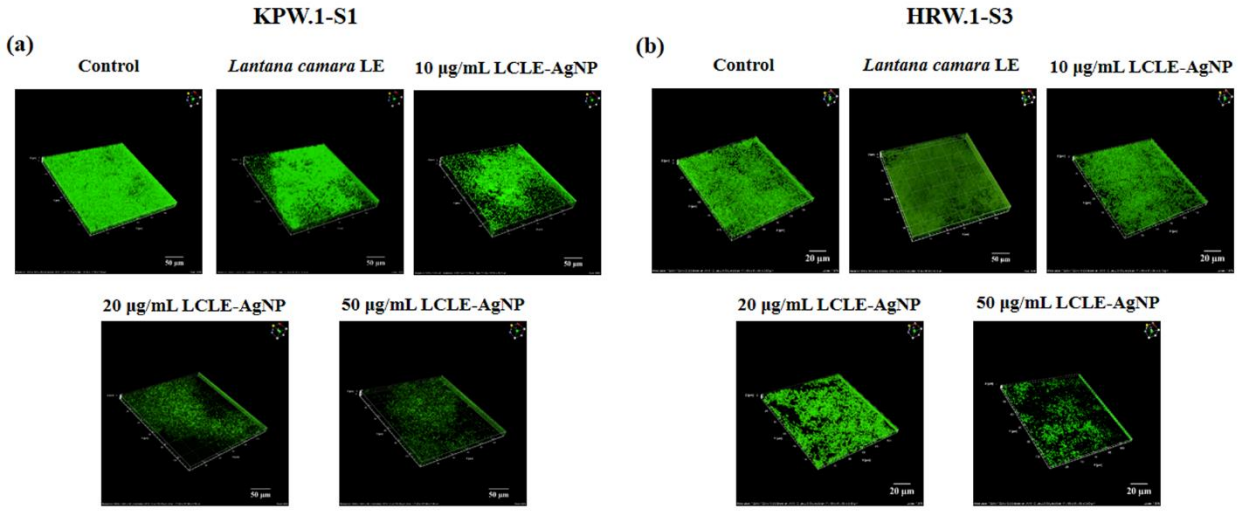

Fig. 8 Representative confocal laser scanning microscopy images of *P. aeruginosa* biofilm in the presence of LCLE-Ag NP. (a) 100X images of KPW.1-S1 biofilm (b) 100X images of HRW.1-S3 biofilm

Figure 9

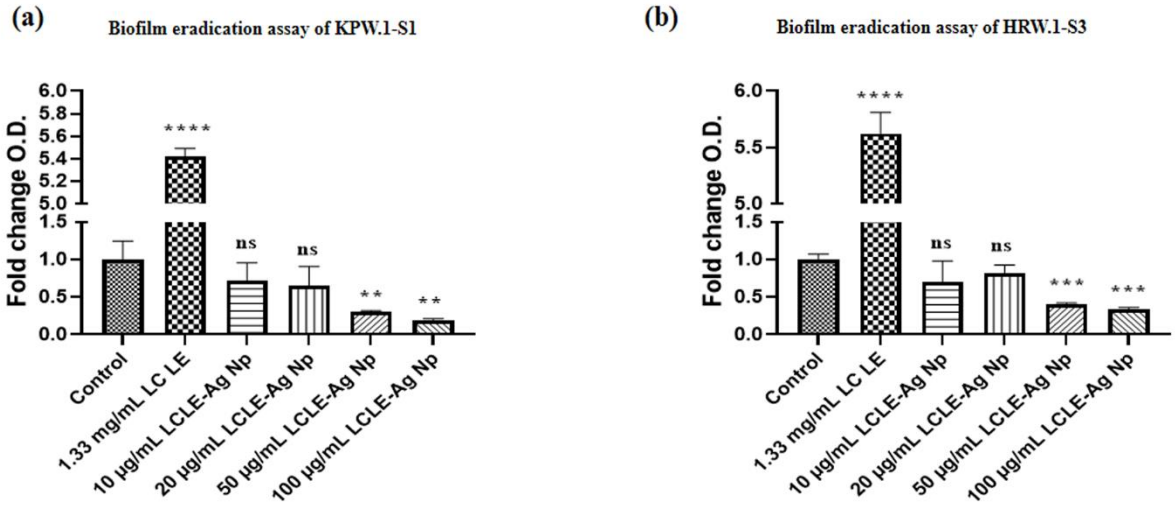

Fig. 9 Biofilm eradication assay of *P. aeruginosa* KPW.1-S1 and HRW.1-S3 in the presence of LCLE-Ag NP. (a) O.D. of biofilm cells of KPW.1-S1 (b) O.D. of biofilm cells of HRW.1-S3; Data represent mean ± SEM of n=9; N=3; *, P ≤ 0.05, **P ≤0.01, ***P ≤0.001, ****P ≤0.0001, while 'ns' indicates non-significance

Figure 10

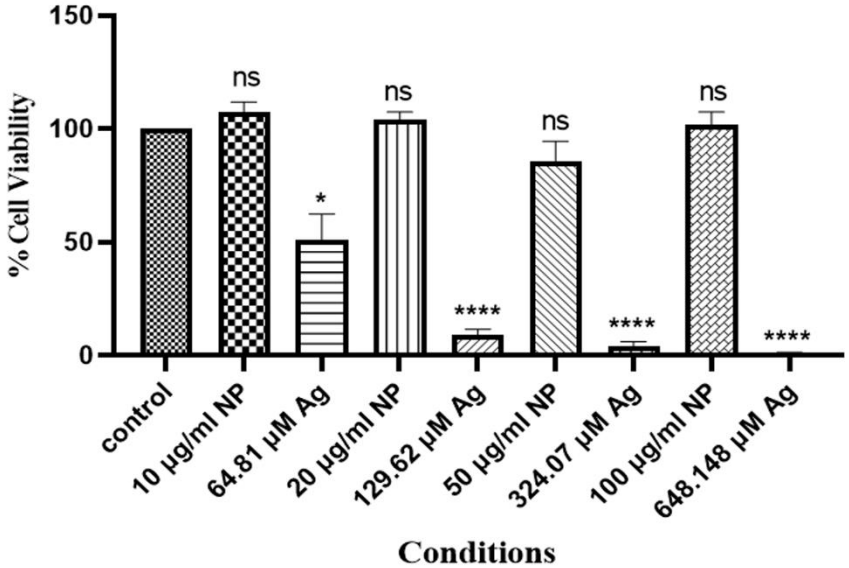

Fig. 10 Quantification of viable cells by MTT assay in HEK293T cells in the presence of LCLE-Ag NPs and its equivalent silver concentration; Data represent mean ± SEM of n=9; N=3; *, P ≤ 0.05, **P ≤0.01, ***P ≤0.001, ****P ≤0.0001